Temporal Variations of Seismicity Rates and Gutenberg–Richter *b*-Values for a Stochastic Declustered Catalog: An Example in Central Italy

Anna Eliana Pastoressa[1], Maura Murru[1], Matteo Taroni[1], Rodolfo Console[*1,2], Caterina Montuori[1], Giuseppe Falcone[1], and Raffaele Di Stefano[1]

Abstract

One important aspect of the seismicity is the spatiotemporal clustering; hence, the distinction between independent and triggered events is a critical part of the analysis of seismic catalogs. Stochastic declustering of seismicity allows a probabilistic distinction between these two kinds of events. Such an approach, usually performed with the epidemic-type aftershock sequence (ETAS) model, avoids the bias in the estimation of the frequency–magnitude distribution parameters if we consider a subset of the catalog, that is, only the independent or the triggered events. In this article, we present a framework to properly include the probabilities of any event to be independent (or triggered) both in the temporal variation of the seismic rates and in the estimation of the *b*-value of the Gutenberg–Richter law. This framework is then applied to a high-definition seismic catalog in the central part of Italy covering the period from April 2010 to December 2015. The results of our analysis show that the seismic activity from the beginning of the catalog to March 2013 is characterized by a low degree of clustering and a relatively high *b*-value, whereas the following period exhibits a higher degree of clustering and a smaller *b*-value.

Cite this article as Pastoressa, A. E., M. Murru, M. Taroni, R. Console, C. Montuori, G. Falcone, and R. Di Stefano (2023). Temporal Variations of Seismicity Rates and Gutenberg–Richter *b*-Values for a Stochastic Declustered Catalog: An Example in Central Italy, *Seismol. Res. Lett.* **94**, 1566–1578, doi: 10.1785/0220220298.

Supplemental Material

Introduction

The seismic hazard assessment and, in general, the capability of identifying possible correlations between the variations of the Earth crust physical properties and the space–time seismicity distribution needs a reliable statistical analysis of the seismic catalogs. The possibility of performing reliable statistical analyses is certainly related to the use of estimation methods that must be robust and independent of the researcher's subjective choices; for this reason, we propose a series of procedures of seismic catalogs' analyses characterized by a high degree of objectivity and robustness, finalized to the estimation of the seismicity rates and Gutenberg–Richter *b*-values (Gutenberg and Richter, 1944) temporal variations.

A first essential step to conduct a careful and conscious study of the seismicity, in addition to a deep knowledge of the catalog and its problems (e.g., catalog completeness), is represented by the so-called declustering process. The declustering process consists in the separation of the independent events from the earthquakes, which depend on each other's (triggered events). This distinction is mainly finalized to collect different information about the earthquake potential estimation. In fact, although independent earthquakes are generally associated with secular tectonic phenomena, the triggered events are mainly attributed to stress variations caused by the previous events (Aki, 1956; Knopoff, 1964).

Currently, there are several approaches for declustering a seismic catalog. In the seismological literature, the most used techniques can be divided into four big categories: window-based methods (e.g., Utsu, 1969; Knopoff and Gardner, 1972; Gardner and Knopoff, 1974; Keilis-Borok and Kossobokov, 1986), link-based methods (e.g., Savage, 1972; Reasenberg, 1985; Frohlich and Davis, 1990; Davis and Frohlich, 1991), stochastic methods (e.g., Kagan and Jackson, 1991; Zhuang *et al.*, 2002; Console, Jackson, and Kagan, 2010), and correlation metric methods (e.g., Baiesi and Paczuski, 2004, 2005; Zaliapin *et al.*, 2008; Zaliapin and Ben-Zion, 2013a, 2013b).

These methods are mainly distinguished by the different models used to characterize the independent events. In detail,

1. Istituto Nazionale di Geofisica e Vulcanologia (INGV), Rome, Italy, https://orcid.org/0000-0002-7385-394X (MM); https://orcid.org/0000-0001-6999-4590 (MT); https://orcid.org/0000-0001-5128-0637 (RC); https://orcid.org/0000-0001-8079-8451 (CM); https://orcid.org/0000-0002-2554-4421 (GF); https://orcid.org/0000-0003-3489-7453 (RDS); 2. Center of Integrated Geomorphology for the Mediterranean Area, Potenza, Italy

*Corresponding author: annaeliana.pastoressa@ingv.it

the window-based, the link-based, and the correlation metric methods have a deterministic and dichotomic approach in the different attributes' selection, classifying an earthquake as either a mainshock or an aftershock or considering a priori values for the parameters in the Gutenberg–Richter scaling law.

On the other hand, in the stochastic approaches, the background seismicity separation from the clustering components is executed starting from the attribution of probability for each event being triggered by another previous event or being an independent event. In the algorithm proposed for the first time by Zhuang *et al.* (2002), these probabilities are computed through the background intensity estimation, considered as a space function constant with time, and through the definitions of parameters associated with the clustered structures obtained by the epidemic-type aftershock sequence (ETAS) model. Although the choice of the best declustering approach is related to the specific pursued goals and to the catalog features (e.g., epicenter and source depth distributions, van Stiphout *et al.*, 2012), the stochastic methods present an approach that avoids subjective choices. Such objectivity makes these methods more reliable than the deterministic methods, which assume arbitrary values for some declustering parameters definition, such as the space–time distance in which mainshocks act.

Moreover, as reported in the work of Mizrahi *et al.* (2021), the ETAS declustering processes appear to be the only declustering algorithms able to avoid bias in the *b*-value estimation for the declustered catalogs. The *b*-values are in fact strongly underestimated when the catalog declustering is executed using window-based and link-based methods (e.g., Marzocchi and Taroni, 2014; Azak *et al.*, 2018; Mizrahi *et al.*, 2021).

However, a correct and reliable seismicity rate and *b*-value estimation will also be related to the definition of the separation criterion to be used to attribute the different probabilities obtained by the stochastic declustering processes to the background and triggered contributes. Generally, in many studies these contributions are separated by choosing a threshold probability of independence (or triggered), with a purely subjective approach to the problem (e.g., Pintori *et al.*, 2021). Instead, in other cases more complicated procedures have been shown: for example, in the work of Ueda and Kato (2019), the background rate is obtained by averaging the different background rates built starting from a big number of stochastic declustered catalogs.

In this article, we adopt an easier strategy for the definition of the independent and triggered seismicity rates, based on the sum of the probabilities for the seismic events to be independent or triggered, respectively. Such probabilities can also be used as weights to perform the *b*-value estimation for the background seismicity and for the clustered seismicity (Zhuang *et al.*, 2002). Therefore, by associating the weights obtained by the stochastic declustering with robust *b*-value estimation methods (Taroni, Vocalelli, and De Polis, 2021), it is possible to build *b*-value time series characterized by a high degree of reliability. For this work, we considered an Italian high-resolution catalog of natural seismicity, recorded by the TABOO (The Alto Tiberina Near Fault Observatory) multidisciplinary research infrastructure managed by the Istituto Nazionale di Geofisica e Vulcanologia (INGV) (see the Dataset section) (Chiaraluce *et al.*, 2014). Starting from this catalog, we have built seismicity rates and Gutenberg–Richter *b*-values time series using the declustering algorithm based on the ETAS-2D model by Console, Murru, and Falcone (2010).

Data

Dataset

TABOO is a part of the community of the Near Fault Observatories (NFOs) that was built within the FP7 European project NERA (Network of European Research Infrastructures for Earthquake Risk Assessment and Mitigation) (2010–2014). This community presently consists of six multidisciplinary research infrastructures operating in regions characterized by high seismic hazard. The NFOs are now part of the European Plate Observing System—Thematic Communities (Chiaraluce *et al.*, 2022). NFOs collect multiparametric near-fault data providing both raw data and advanced scientific products through the EPOS-related services. The TABOO target area is located along the upper Tiber Valley (northern Apennines of Italy, see Fig. 1) where the Alto Tiberina fault (ATF), an east-dipping low-angle normal fault (dip 15°–25°), dominates at depth an extensional fault system active in the Quaternary (Barchi *et al.*, 1998; Pialli *et al.*, 1998; Boncio *et al.*, 2000; Mirabella *et al.*, 2011; Chiaraluce *et al.*, 2014). This area perfectly fits the basic rules for being an NFO: it hosts active faults, it is relatively small, and it is characterized by a relatively high seismicity. As this area was chosen as an NFO, the Italian National Seismic Network held by INGV was here progressively complemented with additional permanent seismic stations since January 2009, adjuvated by a short-term experiment (24 temporary stations were active between April 2010 and February 2011), and it was also progressively instrumented with several other multidisciplinary monitoring systems.

The INGV seismic network in the TABOO area before the NFO implantation consisted of 26 stations with minimum and median interdistances of 6 km and 71 km, respectively (see Fig. 1), whereas excluding the temporary stations, it now consists of 55 stations with minimum and median interdistances of 1 km and 50 km, respectively, since 2010. Nevertheless, it is worth noting that the stations characterized by interdistances as small as 10–30 km are prevalent within the network. This greatly improves the locations' quality, especially of the depth, keeping the closer station distance low. The catalog used in the present article was built by combining in a fully automatic workflow (Di Stefano *et al.*, 2014), a sensitive events detection, a high quality, *P*- and *S*-onset picking and weighting system

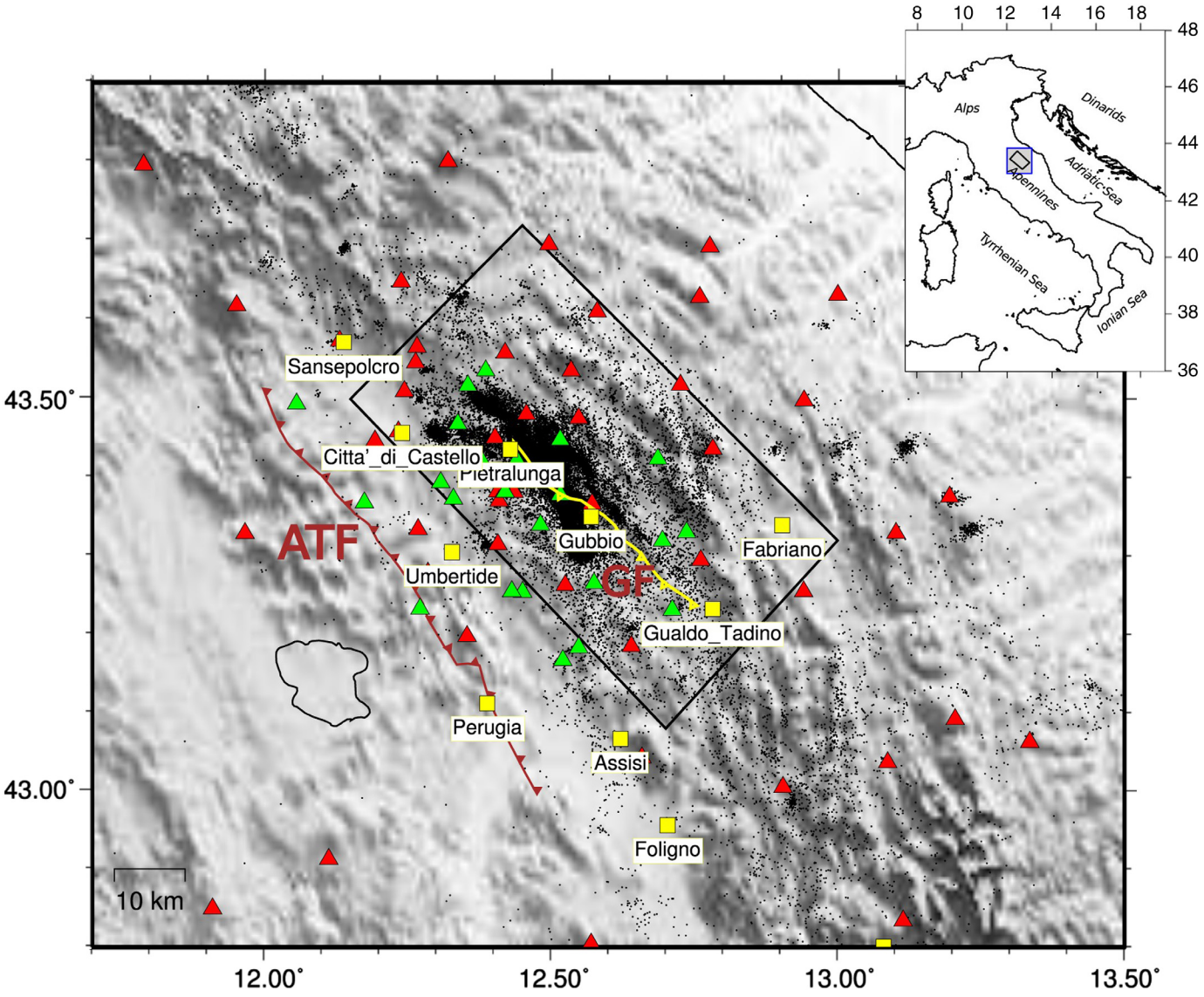

Figure 1. Epicentral distribution of all events falling within The Alto Tiberina Near Fault Observatory (TABOO) area in the time period 1 April 2010–5 December 2015. The black polygon highlights the analyzed area. The Alto Tiberina fault (ATF) and Gubbio fault (GF) are shown with red and yellow lines, respectively. The main municipalities are also indicated with yellow squares. The red and green triangles show permanent and temporary stations, respectively. The inset map shows the location in Italy of this figure. The color version of this figure is available only in the electronic edition.

(Di Stefano *et al.*, 2006; Aldersons *et al.*, 2018), a local tomographic 3D velocity model built on purpose for the automatic workflow (Di Stefano *et al.*, 2014), and a robust 3D tomographic and location code (SimulPS, Thurber, 1983; Eberhart-Phillips, 1986, 1990). Finally, the resulting ∼135k earthquakes were quality selected for root mean square (≤0.3), number of phases (≥10), maximum gap (≤270), maximum horizontal and vertical location errors (≤1.5 km), and minimum number of stations with M_L estimation (≥5). The final dataset consists of ∼50k high-quality located earthquakes from April 2010 to December 2015. M_L is calculated, for each event, as the median (with related standard deviation) over all the available stations' M_L. Stations' M_L are calculated by applying a derived attenuation law for the TABOO zone (Marzorati and Cattaneo, 2016) to the mean of the two horizontal channels' amplitude. Amplitudes in their turn are automatically estimated as the maximum peak-to-peak elongation of the signal after the convolution to standard Wood–Anderson sensor. A specificity of the applied method is the use of an adaptive band-pass prefiltering. The algorithm automatically finds the optimum lower and upper corner frequency for the specific channel seismogram (sensor-earthquake couple) in the frequency range where signal-to-noise ratio is higher (over a given threshold of 5), so to better preserve also the signal of smaller magnitude events.

The maximum elongation is searched in a window extending from the automatic *P* arrival to 5 s beyond the automatic or

TABLE 1
Strongest Events with $M_L \geq 3.5$ in the Area Drawn from the Polygon (Fig. 1)

Province	Date (yyyy/mm/dd)	Latitude (°)	Longitude (°)	Local Magnitude (M_L)	Depth (km)
Pietralunga (PG)	2010/04/15	43.47	12.43	3.5	4.09
Gubbio (PG)	2013/12/18	43.38	12.52	3.6	3.18
Gubbio (PG)	2013/12/22	43.38	12.51	3.8	3.72

theoretical *S*-arrival time. The combination of the TABOO dense seismic network and the use of this adaptive filtering approach allowed a very low threshold in seismic event detection (M_L around 0.2) and a very low completeness magnitude of the catalog ($M_c = 0.5\ M_L$).

Catalog analysis and completeness magnitude estimation

The high-resolution TABOO catalog contains inside the volume (latitude 42.6°–44.2°N/longitude 11.5°–35.5°E) (−1.5 < depth (km) < 34.16) 50,483 events from 1 April 2010 up to 5 December 2015, the last date on which the catalog was updated. The TABOO catalog reports an abundance of small earthquakes that can help better understand the fundamental scaling laws of statistical seismology. The magnitude range starts from −2.77 M_L to a maximum magnitude equal to 4.01 obtained for the 28 August 2010 earthquake with coordinates 12.670°E–42.831°N at a depth of 7 km occurred 14 km south of Foligno (Perugia) (Fig. 1). The check of the quarry blasts inside the area by the catalog of Non-Tectonic Source EarthQuakeS (NTSEQS, Ladina *et al.*, 2021) in central-eastern Italy, shows 191 artificial events that were removed from the dataset.

We focus our analysis inside the polygon, shown in Figure 1, which contains the major part of the seismicity along the Alto Tiberina low-angle normal fault system (ATF) and Gubbio fault (GF). In Table 1, the events with $M_L \geq 3.5$ are reported. The analysis of the events in depth shows that the major part of the seismicity is contained down to 15 km and as an additional check to be sure that we have deleted all the quarry blasts, we only analyze the dataset inside the depth range between 0.5 and 15.0 km.

One of the most important parameters for the statistical analysis of seismicity (and in particular the *b*-value) is the determination of the catalog's minimum completeness magnitude M_c. Different techniques have been suggested to estimate M_c, such as the entire magnitude range method, the maximum curvature method, goodness-of-fit test, and M_c by *b*-value stability (e.g., Rydelek and Sacks, 1989; Ogata and Katsura, 1993; Wiemer and Wyss, 2000; Cao and Gao, 2002).

We follow the approach suggested by Herrmann and Marzocchi (2021), because it is a conservative technique to determine the M_c of high-resolution earthquake catalogs. Consequently, we use the Lilliefors test (Lilliefors, 1969) as a statistical goodness-of-fit test with the exponential distribution to determine the lowest magnitude cut-off, above which the magnitude is exponentially distributed. In other words, above $M_c^{\text{Lilliefors}}$, the frequency–magnitude distribution (FMD) is consistent with the exponential-like Gutenberg–Richter relation. The *p*-value expresses the probability to observe the data sample assuming that the exponential distribution is true. We use a *p*-value with a significance level of $p = 0.1$, conservative in a statistical sense (Clauset *et al.*, 2009) to obtain the lowest magnitude level above which the FMD can be considered exponential.

In Figure 2, the results of this analysis are reported. For our dataset (1 April 2010–5 December 2015) we obtain an $M_c^{\text{Lilliefors}} = 0.5$ with a total of 6531 events (0.5 < depth [km] ≤ 15.0), which will be the dataset that we will use for subsequent analyzes. Further details about the completeness magnitude computation and its influence on the *b*-value estimation are reported in the supplemental material, available to this article, Texts S1 and S2, respectively.

Methods

ETAS 2D model

The model applied in this study is based on the ETAS method and is used for an epicentral analysis (2D) of seismicity where depth has not been taken into account (ETAS 2D) (see e.g., Ogata, 1998, 1999; Console and Murru, 2001; Console *et al.*, 2003).

ETAS is a point process model that assumes the earthquake sequence is made up of aftershocks and background events. Aftershocks include those events that are triggered by other earthquakes whereas the background events are those that occur independent of other earthquakes. A few basic power laws, typical of complex systems are used: (1) the Omori–Utsu (Utsu, 1961; Ogata, 1983) for the temporal decay of the triggered events and (2) the Utsu–Seki (Utsu and Seki, 1955) that describes the dependence of the number and spatial distribution of triggered earthquakes with the mainshock magnitude (see also Kanamori and Anderson, 1975).

One of the most remarkable features of such a model is that the magnitude of the triggered earthquakes is randomly sampled from an FMD, usually a Gutenberg–Richter law (Gutenberg and Richter, 1944). This implies no distinction

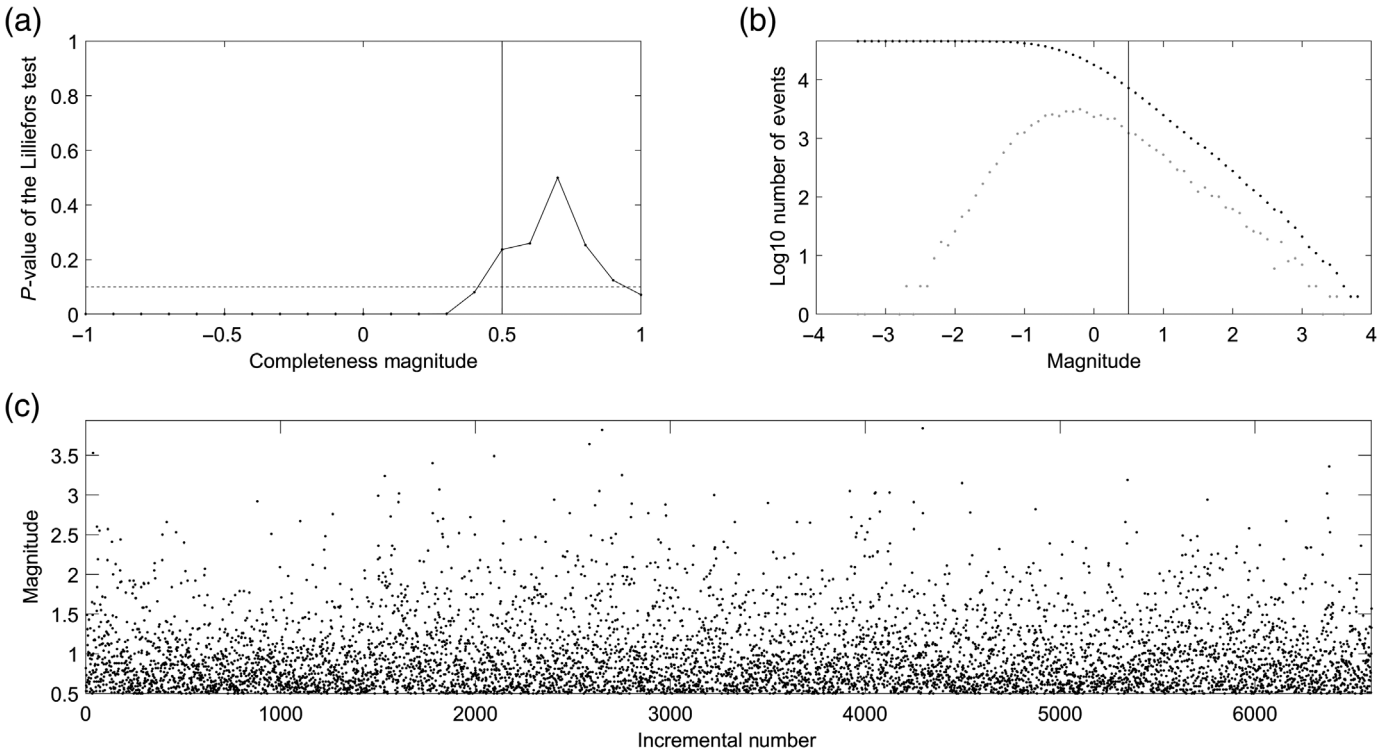

Figure 2. Magnitude distribution for the TABOO catalog inside the polygon shown in Figure 1, for the time period 1 April 2010–5 December 2015. (a) The Lilliefors *p*-value as a function of M_c, considering all the dataset magnitudes. The horizontal dashed line indicates the significance level, 0.1, above which the frequency–magnitude distribution (FMD) can be considered exponential. (b) The magnitude–frequency distribution, considering all the dataset magnitudes. The gray and black dots indicate the exponential distribution and the cumulative number of events, respectively. The vertical line indicates the considered $M_c^{\text{Lilliefors}}$. (c) The sequential number of the events versus the magnitude from 1 to 6.531, which corresponds to the first and last event of the dataset, respectively.

between foreshocks, mainshocks, and aftershocks (e.g., Felzer *et al.*, 2004) that can be identified only "a posteriori." In other words, there is no specific preparatory phase before a large earthquake, because its probability is only proportional to the seismicity rate.

For the model, the expected number of earthquakes above $M_{\min}$ ($M_{\min} \geq M_c^{\text{Lilliefors}}$) in the epicentral space–time unit window, given the observations before time t, at epicentral location $\vec{x}$ can be generically described as follows:

$$\lambda(t,\vec{x}) = \nu\mu(\vec{x}) + \sum_{i:t_i<t} \frac{k}{(t-t_i+c)^p}\left(\frac{(d_0 10^{\alpha(M_i-M_{\min})})^2}{(d_0 10^{\alpha(M_i-M_{\min})})^2 + |\vec{x}-\vec{x}_i|^2}\right)^q, \quad (1)$$

in which ν is a failure rate factor that represents the fraction of spontaneous events (i.e., the ratio between the expected number of independent events and the total number of events, ranging between 0 and 1); $\mu(\vec{x})$ represents the rate density of the long-term average seismicity; t_i defines the occurrence time of earthquakes; k is the productivity coefficient; $c$is the time constant of the Omori law; p is the exponent of the Omori law; q is the exponent of the epicentral spatial distribution of triggered events; d_0 is the epicentral characteristic triggering distance of an earthquake of magnitude $M_{\min}$; M_i is the magnitude of each earthquake considered; and α is the coefficient of the exponential magnitude productivity law.

The epicentral smoothed total time-independent rate-density function $\mu(\vec{x})$ is computed using the method introduced by Frankel (1995), described in detail by Console and Murru (2001) and Console *et al.* (2003). The correlation distance used in the exponential kernel distribution of the smoothing algorithm was found to be 4 km. It was determined by maximizing the likelihood of the seismicity in half of the catalog under the time-independent model obtained from the other half and vice versa.

The expression of the summation in equation (1) represents the triggering kernel that depends on time, space, and magnitude. It considers the contribution of every previous event based upon the magnitude of triggering events, the epicentral spatial distance of triggering earthquakes, and the time interval between the triggering event and the forecast. This part is predominant during a sequence. The free parameters of the model (k, c, p, q, d_0) are estimated by the maximum-likelihood method. The parameter ν is not determined from the best fit in the learning phase, because it is related to all of the other parameters of the model.

TABLE 2
Best-Fit Parameters of the Epidemic-Type Aftershock Sequence (ETAS) 2D Model Optimized over the Study Period (1 April 2010–5 December 2015)

Parameter	Value
Number of events with $M \geq 2.1$	6,531
Lower magnitude threshold of triggering events	0.5
Lower magnitude threshold of target events	0.5
k(days^{p-1}), productivity coefficient	5.34
c(days), time constant in Omori law	0.02
q, exponent of the epicentral spatial distribution of triggered events	2.21
p, exponent in Omori law	1.16
d_0 (km), characteristic triggering distance in the spatial distribution	0.2
ν, fraction of spontaneous events	0.23
$\ln L_1$, maximum log likelihood of the catalog under the clustering hypothesis	96,042.87
$\ln L_0$, maximum log likelihood of the catalog under the Poisson hypothesis	64,127.69
$d \log L = \ln(L_1/L_0)$, log-likelihood ratio	31,915.17

In the second step of the smoothing algorithm, the events receive a weight proportional to the probability of being independent, with a number between 0 (if the event is totally triggered) and 1 (if the event is totally independent) (Console, Jackson, and Kagan, 2010), as in the method introduced by Zhuang *et al.* (2002). These weights were adjusted following an iterative procedure similar to that adopted by Marsan and Longliné (2008). The final maximum-likelihood best-fit parameters of the ETAS model applied to our data set are shown in Table 2.

With this approach it is possible to assign to each event a weight equal to the probability to be independent without the need of removing events from the catalog.

Number of occurrences estimation in time

The strategy here used to separate the seismic occurrences for the different seismicity contributions is based on the probability of an event to be independent and its complementary value, estimated by the ETAS declustering process. In detail, to obtain the occurrence number of independent events (Sb_k) at the k-time window, we considered the sum of independence probabilities (φ_i) for each earthquake until the ith event, as reported in the following equation:

$$Sb_k = \sum_i \varphi_i. \tag{2}$$

In this way the independence probabilities acting as weights will allow us to compute the background occurrences simply by giving a different importance to the different earthquakes recorded in the catalog. The greater the independence probability of an event, the greater its weight in the estimation of background occurrences, and vice versa.

Following the same approach and defying the triggered probability as

$$\rho_i = 1 - \varphi_i, \tag{3}$$

the occurrence number of clustered seismicity at the kth window (Sc_k) will always be expressed as the sum of these probabilities:

$$Sc_k = \sum_i 1 - \varphi_i. \tag{4}$$

This method that allows to quickly separate the number of occurrences of the different components of seismicity appears simple from a mathematical point of view, avoiding any type of subjectivism.

Fourier transform

In this study, to analyze the periodical features of the independent seismicity rate in our dataset, we make use of the definition of the Fourier transform of a time function $f(t)$ as

$$\Im[f(t)] = F(\omega) = \int_{-\infty}^{+\infty} f(t) e^{-i\omega t} \mathrm{d}t, \tag{5}$$

in which i is the imaginary unit.

We apply this definition to the function describing the time history of the seismicity rate by means of a computer code, performing the integral (equation 5) by a numerical discretization. To obtain realistic results, an appropriate discretization has to be chosen for the input and output functions. As $F(\omega)$ is a complex number, we consider just its absolute value $|F(\omega)|$ in the presentation of our results.

Estimation of the *b*-value in time

The estimate of the changes in the b-value was performed by the "weighted likelihood estimation" (WLE) approach (Taroni, Zhuang, and Marzocchi, 2021). According to this method, the b-value estimate at time t, $b(t)$ is performed considering all the events until the time t and attributing to each of them a weight that varies according to the temporal distance with respect to time t (equation 4 in Taroni, Vocalelli, and De Polis, 2021). In this way, avoiding using a fixed number of events, as defined in the classic "rolling window approach" (e.g., Gulia and Wiemer, 2019), and therefore avoiding obtaining time windows of different lengths, it is possible to ensure that only the recent events may be relevant in the estimation of the b-value, thus obtaining a more robust and objective estimation of b-value changes over time. Here, the WLE is used both to properly take

into account the temporal variation of the seismicity and to correctly consider the weights assigned to each event by the stochastic declustering following the technique of Console, Jackson, and Kagan (2010). Indeed, to estimate the *b*-value contributions relating to background ($\hat{b}(t)_{\mathrm{back}}$) and triggered ($\hat{b}(t)_{\mathrm{trig}}$) seismicity, we implemented the WLE algorithm through additional weights as reported in the following equations:

$$\hat{b}(t)_{\mathrm{back}} = \frac{\sum_{i=1}^{n(t)} W(t_0 - t_i)\varphi_i}{\ln(10)\left(\sum_{i=1}^{n(t)} W(t_0 - t_i)\varphi_i (M_i - M_c) + \frac{\Delta M}{2}\right)}, \quad (6)$$

$$\hat{b}(t)_{\mathrm{trig}} = \frac{\sum_{i=1}^{n(t)} W(t_0 - t_i)\rho_i}{\ln(10)\left(\sum_{i=1}^{n(t)} W(t_0 - t_i)\rho_i (M_i - M_c) + \frac{\Delta M}{2}\right)}, \quad (7)$$

in which $W(t_0 - t_i)\varphi_i$ and $W(t_0 - t_i)\rho_i$ correspond to the weights assigned to each of the $n(t)$ events considered up to time t; $W(t_0 - t_i)$ is the weight that depends on the time lapse between the ith event and the first event in the catalog at time t_0, whereas the weights φ_i and ρ_i are the ones related to the stochastic declustering algorithm, related to the background and triggering probability, respectively; M_i is the magnitude of the ith event, ΔM is the magnitude binning, and M_c is the magnitude of completeness of the catalog. Then, using equations (6) and (7), it is possible to estimate the temporal variations of the *b*-value for the background and triggered events in the catalog, separately.

Such an approach also avoids the subjective choice of the number of events used for the temporal estimation of the *b*-value (usually 100 or 200 events, Taroni, Vocalelli, and De Polis, 2021). The importance of recent events with respect to the earlier is controlled by the weight $W(t_0 - t_i)$, defined as $W(t_0 - t_i) = \exp(-\alpha\Delta T)$, in which ΔT corresponds to time lapse between the ith event and the first event in the catalog, and α is the parameter that regulates the amount of past information relevant in the estimation (this last parameter is objectively estimated with the maximum-likelihood approach, as explained in Taroni, Vocalelli, and De Polis, 2021). With respect to the equations of Taroni, Vocalelli, and De Polis (2021), here we used nonnormalized weights, because our weights are composed by two different factors, then the numerator of equations (6) and (7) is not equal to 1 but is equal to the sum of all the weights considered in the computation.

Results

In this section, we present the time series both of seismic rate and Gutenberg–Richter *b*-value for the TABOO catalog, starting from the ETAS 2D model, composed by 6523 events recorded from 11 April 2010 to 5 December 2015. The earthquakes recorded from 1 to 10 April 2010 were not used for this analysis due to the so-called "warm-up" phenomenon, consisting in an unrealistic high probability of independence of the events in the initial part of the catalog, due to the omission of previous triggering earthquakes. The ETAS model, in fact, associates an independence probability equal to 1 to all those events without information on foreshocks. Therefore, to ensure data stability, the first 10 days of the TABOO catalog have been removed.

For the seismic rate analysis, we considered not only the daily variation of the event number that occurred in the whole TABOO catalog, but also the changes related to the background and triggered components. As mentioned earlier, the separation of the different contributions was possible through the independence probability values obtained from the ETAS declustering algorithm by Console, Jackson, and Kagan (2010). In detail, summing the independence probability (φ_i) (by equation 2) and the triggered probability (ρ_i) (by equation 4), we have obtained the background and triggered daily seismic rates, respectively. The results of these computations are shown in Figure 3.

Observing the incremental and cumulative event number distribution in time we can note a twofold behavior in the earthquake occurrence. The first part of the catalog, from April 2010 to about March 2013, is in fact characterized by a low number of events (about 1456) with an occurrence of about 1.4 earthquakes per day. Moreover, in this time lapse the number of background and triggered events (about 713 and 743, respectively) appears very similar.

Instead, in the last years, from March–April 2013 to December 2015, the seismicity rate increased sharply and the largest daily variation has been recorded, with the average occurrence of about 6.5 events per day in a small-time interval from March 2013 to October 2014 (seismic swarms). This earthquake frequency increase appears to be closely related to the triggered events whose number is equal to 4299 in the second part of the catalog, reaching a maximum value of about 3522 events during the year ranging between 2013 and 2014. On the other hand, though in the last few years the background seismicity is still characterized by a low number of earthquakes (about 772), also for this component the maximum number of occurrences results concentrated during the seismic swarms of 2013–2014, which mainly affected the municipalities of Città di Castello, Gubbio, and Pietralunga.

The seismic background highlights small variations, which are better visible by analyzing the seismicity rate with a bigger observation window. In fact, observing the monthly behavior of the background (Fig. 4a), the nonstationarity of this component appears evident, showing two maximum values: one at the beginning of 2011 and the other one in the second-half of 2014.

This trend is clearly shown also with a quantitative approach through Fourier transform executed for the background events, for which the maximum frequency is defined for a time period of about 40 months (peak at 0.025 in Fig. 4b).

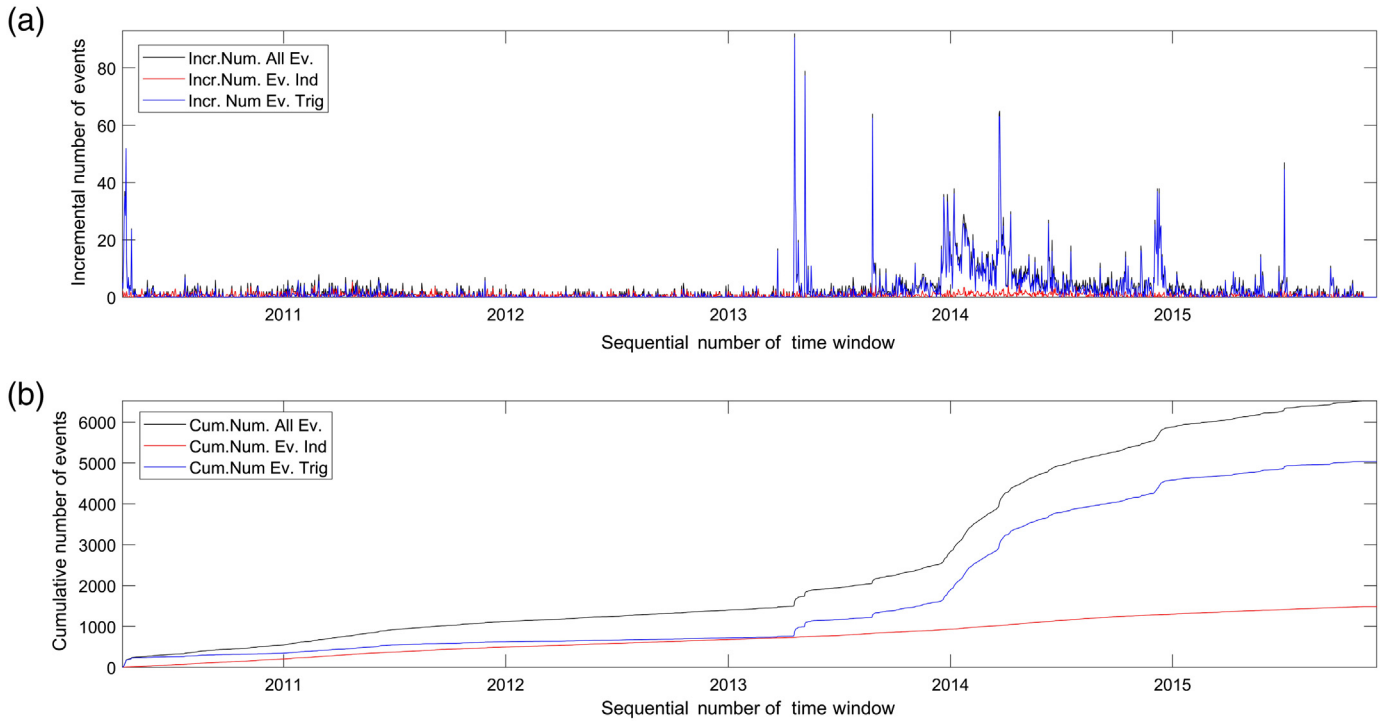

Figure 3. (a) Incremental number and (b) cumulative number of events daily recorded in the TABOO catalog from 11 April 2010 to 5 December 2015. The black, red, and blue lines indicate the entire earthquake in the catalog, the independence and triggered events, respectively. The color version of this figure is available only in the electronic edition.

Given the short duration of the recording of the seismic catalog (5 yr) with respect to the oscillation period detected (40 months), whether such variations are linked to a real periodic behavior of the background or whether the maximum occurrence values are due to transient phenomena appears not simple to understand.

For the *b*-value analysis, as in the previous analysis, we consider the time series of the whole TABOO catalog, and also the changes related to the background and triggered components separately. The results of the estimations are reported in Figure 5a, for which the black, red, and blue lines indicate the *b*-value time series for the whole catalog, for the background seismicity and for triggered events, respectively. These curves were built estimating forgetting parameter $\alpha = 0.020$ for our catalog. Further information about the *b*-values estimation errors in terms of standard deviations are available in Text S3.

Observing the curves reported earlier, we can note that for the entire duration of the recording, the *b*-values estimated considering all the events of the TABOO catalog are ranging between the *b*-values of the background events (higher) and the *b*-values of the triggered events (lower). In particular, this gap between the different *b*-values appears to be very small in the first three years of the catalog, from April 2010 to about March–April 2013, for which the *b*-average values are near to 1.1 for both the entire catalog and for the different components of the seismicity.

As clearly highlighted by the distribution of magnitude over time (Fig. 5b), the number of events recorded in these first three years is very low, about one-sixth of that reported in the entire catalog. However, starting from April 2013, the different behavior between the *b*-values of background and *b*-values of triggered seismicity appears more evident. In fact, for the background events the *b*-values oscillate always around an average of about 1.1, whereas for the triggered events the *b*-values show a sharp reduction reaching average values of about 0.8–0.9.

This different behavior of *b*-values estimated for the different components of seismicity is in line with the observations of Chiaraluce *et al.* (2007) and Valoroso *et al.* (2017), which mainly attribute this difference to the different structures responsible to generate independent events or triggered events. According to these authors, in fact, although the background seismicity is mostly attributable to the low-angle ATF, for which a number of events homogeneously distributed in time and space are evident, the triggering seismicity, characterized by multiple seismic sequences recorded mainly starting from April 2013 (Fig. 5b), should instead be associated with the activity of the synthetic and antithetic faults placed on the ATF hanging wall.

Therefore, in the geological framework of the ATF system, the global *b*-value appears strongly affected by the triggered seismicity, which is predominant in this study area, with a number of events equal to about 5042 out of a total number of 6523 events recorded. It is in progress a work that will

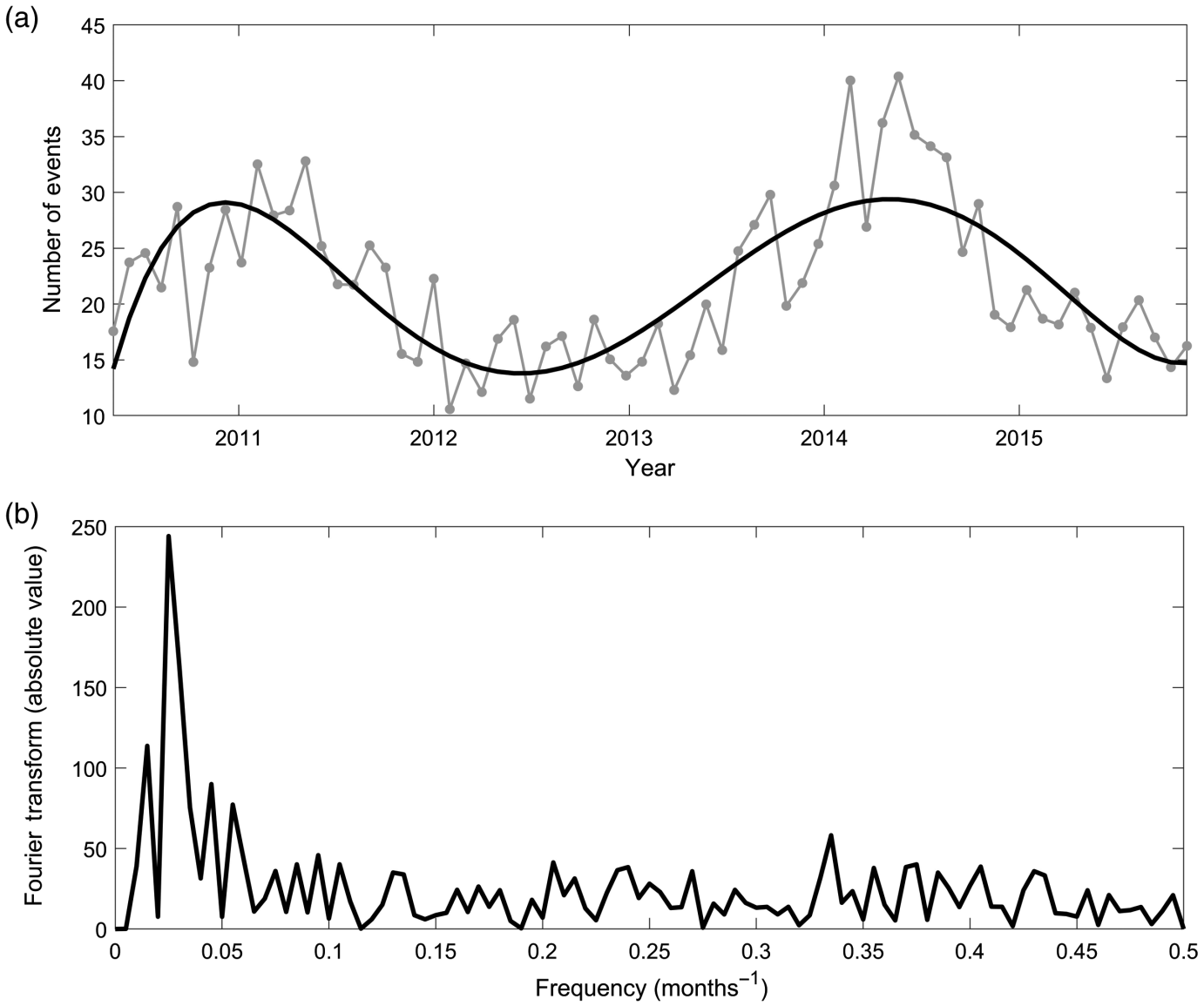

Figure 4. (a) Estimated number of background events occurred monthly (30 days) and (b) frequency spectrum of the background seismicity computed through the Fourier transform.

examine the time and space variations of the seismicity rates and the Gutenberg–Richter *b*-values for the ATF system, also taking in account the depths of events recorded in the TABOO catalog, through the construction of a new ETAS 3D model.

Conclusions

As demonstrated by numerous studies (e.g., Scholz, 1968, 2015; Wiemer and Wyss, 1997; Wiemer *et al.*, 1998; Oncel and Wyss, 2000; Wyss *et al.*, 2001; Murru *et al.*, 2005, 2007; Schorlemmer *et al.*, 2005; Meletti *et al.*, 2008; Bachmann *et al.*, 2012; Tormann *et al.*, 2014, 2015), *b*-values fluctuations could be related with physical proprieties and dynamism of the Earth crust. In particular, the recent work of Gulia and Wiemer, (2019) highlighted how the *b*-value temporal evolution could have a predictive meaning in the upcoming large-event occurrence. For these reasons, reliable computation of the *b*-value time series represent an important instrument for a specific zone in the seismic hazard assessment. Therefore, in this work, we wanted to present a series of procedures finalized to an objective analysis of seismic catalogs to minimize biases in the *b*-value temporal variation estimation for background and clustered seismicity. In detail, to separate the different contributions of seismicity we proposed a new approach for the analysis of stochastic declustered catalogs based on the use of weights obtained from the independence probabilities, achieved through the construction of the ETAS 2D model. Thanks to our simple but rigorous approach that applies a criterion not affected by subjective choices, the estimation of the seismic rates and Gutenberg–Richter *b*-value time variations both for independence and triggered earthquakes is possible.

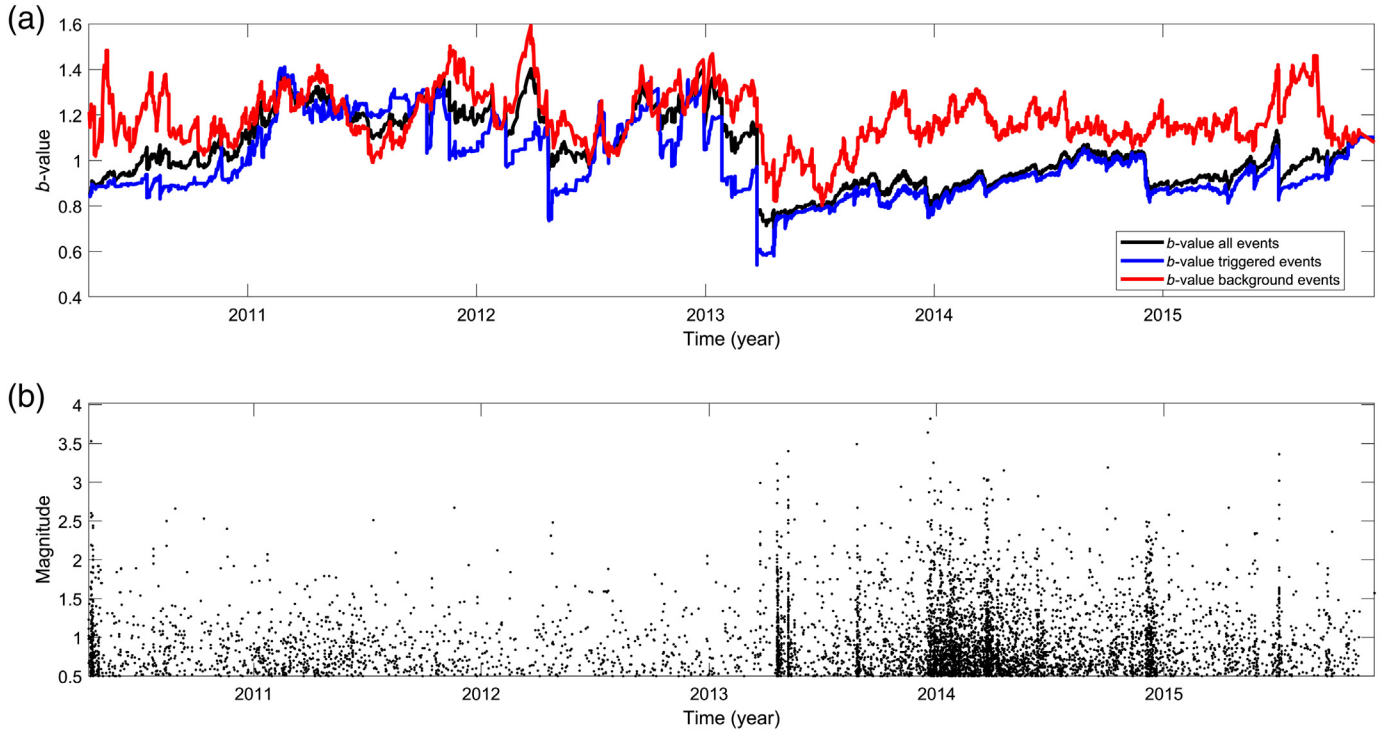

Figure 5. (a) *b*-value time series estimated using the weighted likelihood approach. The black line refers to all events recorded in the TABOO catalog, whereas the red line and the blue line are the *b*-values for background and clustered seismicity, respectively. (b) Magnitude earthquakes distribution over time. The color version of this figure is available only in the electronic edition.

For demonstration purposes, we applied this study to a high-resolution catalog. However, the procedures shown can also be used for classical instrumental seismic catalog. In detail, this analysis executed on TABOO catalog allowed to separate the background and clustered contributions for the Alto Tiberina seismic area, highlighting how the variations in the seismic rates and in the *b*-values are mainly related to the triggered events that appear predominant in terms of number of occurrences in the considered time period. Moreover, the seismic rate time-series analysis puts in evidence the nonstationarity for background seismicity, in which the biggest oscillations showed mostly a three-years frequency. Regarding the *b*-value time-series analysis, the estimations suggested a higher *b*-value for background events with respect to triggered events.

Data and Resources

The dataset considered in this work is generated by The Alto Tiberina Near Fault Observatory (TABOO), an Istituto Nazionale di Geofisica e Vulcanologia (INGV) monitoring infrastructure. This infrastructure is part of the European Plate Observing System—Implementation Phase (EPOS-IP) project, available at http://www.epos-eu.org, which received funding from the European Union's Horizon 2020 research and innovation program under Grant Agreement Number 676564. Quarry blasts analysis was executed considering the "Catalog of non-tectonic earthquakes in Central-Eastern Italy" redacted from the Ancona section of the INGV available at http://www.an.ingv.it/NTSEQS. The *b*-value time series built through the "weighted likelihood approach" (WLA) were obtained using the code by Taroni, Vocalelli, and De Polis (2021) available at –https://github.com/MatteoTaroniINGV/Bvalue_TimeSeries_WeightedLikelihoodEstimation. All the graphs reported in the figures were made using MATLAB codes. Figure 1 was made using Generic Mapping Tools (GMT) software (Wessel *et al.*, 2013). The supplemental material for this article includes further information about the reliability of *b*-value time-series estimation. In particular, we focused on (a) the magnitude of completeness estimation, (b) the influence of changes in completeness magnitude on the *b*-value time series, and on (c) the computation of *b*-values standard deviations. All websites were last accessed September 2022.

Declaration of Competing Interests

The authors declare that there are no conflict of interests recorded.

Acknowledgments

This work was supported by the 2020–2023 Istituto Nazionale di Geofisica e Vulcanologia (INGV) Department Strategic Project named MUSE (Multiparametric and mUltiscale Study of Earthquake) preparatory phase in the central and northern Apennines. The authors wish to thank the two reviewers for their valuable comments. The authors also thank the editors of *SRL* for their support and encouragement.

References

Aki, K. (1956). Some problems in statistical seismology, *Zisin* **8,** 205–228, English translation by A. S. Furumoto, Univ. of Hawaii (1963), doi: 10.4294/zisin1948.8.4_205 (in Japanese).

Alderson, D. L., G. G. Brown, W. M. Carlyle, and R. K. Wood (2018). Assessing and improving the operational resilience of a large highway infrastructure system to worst-case losses, *Transp. Sci.* **52,** no. 4, 1012–1034, doi: 10.1287/trsc.2017.0749.

Azak, T. E., D. Kalafat, K. Şeşetyan, and M. B. Demircioğlu (2018). Effects of seismic declustering on seismic hazard assessment: A sensitivity study using the Turkish earthquake catalogue, *Bull. Earthq. Eng.* **16,** no. 8, 3339–3366, doi: 10.1007/s10518-017-0174-y.

Bachmann, C., S. Wiemer, B. Goertz-Allmann, and J. Woessner (2012). Influence of pore-pressure on the event-size distribution of induced earthquakes, *Geophys. Res. Lett.* **39,** L09302, doi: 10.1029/2012GL051480.

Baiesi, M., and M. Paczuski (2004). Scale-free networks of earthquakes and aftershocks, *Phys. Rev. E* **69,** no. 6, 066106, doi: 10.1103/PhysRevE.69.066106.

Baiesi, M., and M. Paczuski (2005). Complex networks of earthquakes and aftershocks, *Nonlin. Process. Geophys.* **12,** no. 1, 1–11, doi: 10.5194/npg-12-1-2005.

Barchi, M. R., A. De Feyter, M. Magnani, G. Minelli, G. Pialli, and B. M. Sotera (1998). Extensional tectonics in the Northern Apennines (Italy): Evidence from the CROP 03 deep seismic reflection line, *Mem. Soc. Geol. Ital.* **52,** 528–538.

Boncio, P., F. Brozzetti, and G. Lavecchia (2000). Architecture and seismotectonics of a regional low-angle normal fault zone in central Italy, *Tectonics* **19,** no. 6, 1038–1055, doi: 10.1029/2000TC900023.

Cao, A. M., and S. S. Gao (2002). Temporal variations of seismic *b*-values beneath northeastern japan island arc, *Geophys. Res. Lett.* **29,** no. 9, 1334, doi: 10.1029/2001GL013775.

Chiaraluce, L., A. Amato, S. Carannante, V. Castelli, M. Cattaneo, M. Cocco, C. Collettini, E. D'Alema, R. Di Stefano, D. Latorre, *et al.* (2014). The Alto Tiberina near fault observatory (northern Apennines, Italy), *Ann. Geophys.* **57,** no. 3, S0327 , doi: 10.4401/ag-6426.

Chiaraluce, L., C. Chiarabba, C. Collettini, D. Piccinini, and M. Cocco (2007). Architecture and mechanics of an active low-angle normal fault: Alto Tiberina fault, northern Apennines, Italy, *J. Geophys. Res.* **112,** no. B10, doi: 10.1029/2007JB005015.

Chiaraluce, L., G. Festa, P. Bernard, A. Caracausi, I. Carluccio, J. Clinton, R. Di Stefano, L. Elia, C. P. Evangelidis, S. Ergintav, *et al.* (2022). The near fault observatory community in Europe: A new resource for faulting and hazard studies, *Ann. Geophys.* **65,** no. 3, DM316–DM316, doi: 10.4401/ag-8778.

Clauset, A., C. R. Shalizi, and M. E. Newman (2009). Power-law distributions in empirical data, *SIAM Rev.* **51,** no. 4, 661–703, doi: 10.48550/arXiv.0706.1062.

Console, R., D. D. Jackson, and Y. Y. Kagan (2010). Using the ETAS model for catalog declustering and seismic background assessment, *Pure Appl. Geophys.* **167,** no. 6, 819–830, doi: 10.1007/s00024-010-0065-5.

Console, R., and M. Murru (2001). A simple and testable model for earthquake clustering, *J. Geophys. Res.* **106,** no. B5, 8699–8711, doi: 10.1029/2000JB900269.

Console, R., M. Murru, and G. Falcone (2010). Retrospective forecasting of M ≥ 4.0 earthquake in New Zealand, *Pure Appl. Geophys.* **167,** 693–707, doi: 10.1007/s00024-010-0068-2.

Console, R., M. Murru, and A. M. Lombardi (2003). Refining earthquake clustering models, *J. Geophys. Res.* **108,** no. B10, doi: 10.1029/2002JB002130

Davis, S. D., and C. Frohlich (1991). Single-link cluster analysis, synthetic earthquake catalogues, and aftershock identification, *Geophys. J. Int.* **104,** no. 2, 289–306, doi: 10.1111/j.1365-246X.1991.tb02512.x.

Di Stefano, R., F. Aldersons, E. Kissling, P. Baccheschi, C. Chiarabba, and D. Giardini (2006). Automatic seismic phase picking and consistent observation error assessment: Application to the Italian seismicity, *Geophys. J. Int.* **165,** no. 1, 121–134, doi: 10.1111/j.1365-246X.2005.02799.x.

Di Stefano, R., L. Chiaraluce, L. Valoroso, F. Waldhauser, D. Latorre, D. Piccinini, and E. Tinti (2014). An automatic modular procedure to generate high-resolution earthquake catalogues: Application to the Alto Tiberina near Fault Observatory (TABOO), Italy, *AGU Fall Meeting Abstracts*, Vol. 2014, T13C–4684, doi: 10.5281/zenodo.1222148.

Eberhart-Phillips, D. (1986). Three-dimensional velocity structure in northern California Coast Ranges from inversion of local earthquake arrival times, *Bull. Seismol. Soc. Am.* **76,** no. 4, 1025–1052, doi: 10.1785/BSSA0760041025.

Eberhart-Phillips, D. (1990). Three-dimensional P and S velocity structure in the Coalinga region, California, *J. Geophys. Res.* **95,** no. B10, 15,343–15,363, doi: 10.1029/JB095iB10p15343.

Felzer, K. R., R. E. Abercrombie, and G. Ekstrom (2004). A common origin of aftershocks, foreshocks, and multiplets, *Bull. Seismol. Soc. Am.* **94,** 88–98, doi: 10.1785/0120030069.

Frankel, A. (1995). Mapping seismic hazard in the central and eastern United States, *Seismol. Res. Lett.* **66,** 8–21.

Frohlich, C., and S. D. Davis (1990). Single-link cluster analysis as a method to evaluate spatial and temporal properties of earthquake catalogues, *Geophys. J. Int.* **100,** no. 1, 19–32, doi: 10.1111/j.1365-246X.1990.tb04564.x.

Gardner, J. K., and L. Knopoff (1974). Is the sequence of earthquakes in Southern California, with aftershocks removed, Poissonian? *Bull. Seismol. Soc. Am.* **64,** no. 5, 1363–1367, doi: 10.1785/BSSA0640051363.

Gulia, L., and S. Wiemer (2019). Real-time discrimination of earthquake foreshocks and aftershocks, *Nature* **574,** 193–199, doi: 10.1038/s41586-019-1606-4.

Gutenberg, B., and C. F. Richter (1944). Frequency of earthquakes in California, *Bull. Seismol. Soc. Am.* **34,** no. 4, 185–188, doi: 10.1785/BSSA0340040185.

Herrmann, M., and W. Marzocchi (2021). Inconsistencies and lurking pitfalls in the magnitude–frequency distribution of high-resolution earthquake catalogs, *Seismol. Res. Lett.* **92,** no. 2A, 909–922, doi: 10.1785/0220200337.

Kagan, Y. Y., and D. D. Jackson (1991). Long-term earthquake clustering, *Geophys. J. Int.* **104,** no. 1, 117–133, doi: 10.1111/j.1365-246X.1991.tb02498.x.

Kanamori, H., and D. L. Anderson (1975). Theoretical basis of some empirical relations in seismology, *Bull. Seismol. Soc. Am.* **65,** no. 5, 1073–1095, doi: 10.1785/BSSA0650051073.

Keilis-Borok, V. I., and V. G. Kossobokov (1986). Time of increased probability for the great earthquakes of the world, *Comput. Seismol.* **19,** 48–58.

Knopoff, L. (1964). The statistics of earthquakes in Southern California, *Bull. Seismol. Soc. Am.* **54,** no. 6A, 1871–1873, doi: 10.1785/BSSA05406A1871.

Knopoff, L., and J. K. Gardner (1972). Higher seismic activity during local night on the raw worldwide earthquake catalogue, *Geophys. J. Int.* **28,** no. 3, 311–313, doi: 10.1111/j.1365-246X.1972.tb06133.x.

Ladina, C., C. Calamita, D. Pantaleo, S. Marzorati, M. Cattaneo, M. Frapiccini, and G. Monachesi (2021). NTSEQS: Catalogue of non-tectonic earthquakes in Central-Eastern Italy, version 2.0 [Data set], *Istituto Nazionale di Geofisica e Vulcanologia (INGV)*, doi: 10.13127/ntseqs2.0.

Lilliefors, H. W. (1969). On the Kolmogorov-Smirnov test for the exponential distribution with mean unknown, *J. Am. Stat. Assoc.* **64,** no. 325, 387–389, doi: 10.1080/01621459.1969.10500983.

Marsan, D., and O. Longliné (2008). Extending earthquakes' reach through cascading, *Science* **319,** 1076–1079, doi: 10.1126/science.1148783.

Marzocchi, W., and M. Taroni (2014). Some thoughts on declustering in probabilistic seismic-hazard analysis, *Bull. Seismol. Soc. Am.* **104,** no. 4, 1838–1845, doi: 10.1785/0120130300.

Marzorati, S., and M. Cattaneo (2016). Stima automatica della magnitudo minima rilevabile dalla rete sismica ReSIICO, *Quaderni di Geofisica* **136,** 21 (in German).

Meletti, C., F. Galadini, G. Valensise, M. Stucchi, R. Basili, S. Barba, G. Vannucci, and E. Boschi (2008). A seismic source zone model for the seismic hazard assessment of the Italian territory, *Tectonophysics* **450,** nos. 1/4, 85–108, doi: 10.1016/j.tecto.2008.01.003.

Mirabella, F., F. Brozzetti, A. Lupattelli, and M. R. Barchi (2011). Tectonic evolution of a low angle extensional fault system from restored cross sections in the northern Apennines (Italy), *Tectonics* **30,** doi: 10.1029/2011TC002890.

Mizrahi, L., S. Nandan, and S. Wiemer (2021). The effect of declustering on the size distribution of mainshocks, *Seismol. Res. Lett.* **92,** 2333–2342, doi: 10.1785/0220200231.

Murru, M., R. Console, G. Falcone, C. Montuori, and T. Sgroi (2007). Spatial mapping of the *b* value at Mount Etna, Italy, using earthquake data recorded from 1999 to 2005, *J. Geophys. Res.* **112,** no. B12, doi: 10.1029/2006JB004791.

Murru, M., C. Montuori, R. Console, and A. Lisi (2005). Mapping of the *b*-value anomalies beneath Mt. Etna, Italy, during July–August 2001 lateral eruption, *Geophys. Res. Lett.* **32,** no. 5, doi: 10.1029/2004GL021545.

Ogata, Y. (1983). Estimation of the parameters in the modified Omori formula for aftershock frequencies by the maximum likelihood procedure, *J. Phys. Earth* **31,** no. 2, 115–124, doi: 10.4294/jpe1952.31.115.

Ogata, Y. (1998). Space-time point-process models for earthquake occurrences, *Ann. Inst. Statist. Math.* **50,** no. 2, 379–402, doi: 10.1023/A:1003403601725.

Ogata, Y. (1999). Seismicity analysis through point-process modeling: A review, *Pure Appl. Geophys.* **155,** 471–507, doi: 10.1007/s000240050275.

Ogata, Y., and K. Katsura (1993). Analysis of temporal and spatial heterogeneity of magnitude frequency distribution inferred from earthquake catalogues, *Geophys. J. Int.* **113,** no. 3, 727–738, doi: 10.1111/j.1365-246X.1993.tb04663.x.

Oncel, A., and M. Wyss (2000). The major asperities of the 1999 Mw=7.4 Izmit earthquake defined by the microseismicity of the two decades before it, *Geophys. J. Int.* **143,** 501–506, doi: 10.1046/j.1365-246X.2000.00211.x.

Pialli, G., M. Barchi, and G. Minelli (1998). Results of the CROP03 deep seismic reflection profile, *Mem. Soc. Geol. Ital.* **52,** 647.

Pintori, F., E. Serpelloni, L. Longuevergne, A. Garcia, L. Faenza, L. D'Alberto, A. Gualandi, and M. E. Belardinelli (2021). Mechanical response of shallow crust to groundwater storage variations: Inferences from deformation and seismic observations in the Eastern Southern Alps, Italy, *J. Geophys. Res.* **126,** no. 2, doi: 10.1029/2020JB020586.

Reasenberg, P. (1985). Second-order moment of central California seismicity, 1969–1982, *J. Geophys. Res.* **90,** no. B7, 5479–5495, doi: 10.1029/JB090iB07p05479.

Rydelek, P. A., and I. S. Sacks (1989). Testing the completeness of earthquake catalogues and the hypothesis of self-similarity, *Nature* **337,** no. 6204, 251–253, doi: 10.1038/337251a0.

Savage, W. U. (1972). Microearthquake clustering near Fairview Peak, Nevada, and in the Nevada seismic zone, *J. Geophys. Res.* **77,** no. 35, 7049–7056, doi: 10.1029/JB077i035p07049.

Scholz, C. H. (1968). The frequency magnitude relation of microfracturing in rock and its relation to earthquakes, *Bull. Seismol. Soc. Am.* **58,** no. 1, 399–415, doi: 10.1785/BSSA0580010399.

Scholz, C. H. (2015). On the stress dependence of the earthquake *b* value, *Geophys. Res. Lett.* **42,** 1399–1402, doi: 10.1002/2014GL062863.

Schorlemmer, D., S. Wiemer, and M. Wyss (2005). Variations in earthquake-size distribution across different stress regimes, *Nature* **437,** 539–542, doi: 10.1038/nature04094.

Taroni, M., G. Vocalelli, and A. De Polis (2021). Gutenberg–Richter b-value time series forecasting: A weighted likelihood approach, *Forecasting* **3,** no. 3, 561–569, doi: 10.3390/forecast3030035.

Taroni, M., J. Zhuang, and W. Marzocchi (2021). High-definition mapping of the Gutenberg–Richter b-value and its relevance: A case study in Italy, *Seismol. Res. Lett.* **92,** no. 6, 3778–3784, doi: 10.1785/0220210017.

Thurber, C. H. (1983). Earthquake locations and three-dimensional crustal structure in the Coyote Lake area, central California, *J. Geophys. Res.* **88,** no. B10, 8226–8236, doi: 10.1029/JB088iB10p08226.

Tormann, T., B. Enescu, J. Woessner, and S. Wiemer (2015). Randomness of megathrust earthquakes implied by rapid stress recovery after the Japan earthquake, *Nature Geosci.* **8,** no. 2, 152–158, doi: 10.1038/ngeo2343.

Tormann, T., S. Wiemer, and A. Mignan (2014). Systematic survey of high-resolution *b*-value imaging along Californian faults: Inference on asperities, *J. Geophys. Res.* **119,** no. 3, 2029–2054, doi: 10.1002/2013JB010867.

Ueda, T., and A. Kato (2019). Seasonal variations in crustal seismicity in San-in district, southwest Japan, *Geophys. Res. Lett.* **46,** no. 6, 3172–3179, doi: 10.1029/2018GL081789.

Utsu, T. (1961). A statistical study of the occurrence of aftershocks, *Geophys. Mag.* **3,** 521–605.

Utsu, T. (1969). Aftershocks and earthquake statistics (1)-Some parameters which characterize an aftershock sequence and their interrelations, *J. Fac. Hokkaido Univ.* **3,** 125–195.

Utsu, T., and A. Seki (1955). Relation between the area of the aftershock region and the energy of the mainshock, *J. Seismol. Soc. Jpn.* **7,** 233–240.

Valoroso, L., L. Chiaraluce, R. Di Stefano, and G. Monachesi (2017). Mixed-mode slip behavior of the Altotiberina low-angle normal fault system (Northern Apennines, Italy) through high-resolution earthquake locations and repeating events, *J. Geophys. Res.* **122,** no. 12, 10–220, doi: 10.1002/2017JB014607.

van Stiphout, T., J. Zhuang, and D. Marsan (2012). Seismicity declustering, *Community Online Resour. Stat. Seism. Anal.* doi: 10.5078/corssa-52382934.

Wessel, P., W. H. Smith, R. Scharroo, J. Luis, and F. Wobbe (2013). Generic mapping tools: Improved version 528 released, *Eos Trans. AGU* **94,** no. 45, 409–410, doi: 10.1002/2013EO450001.

Wiemer, S., and M. Wyss (1997). Mapping the frequency-magnitude distribution in asperities: An improved technique to calculate recurrence times? *J. Geophys. Res.* **102,** 15,115–15,128, doi: 10.1029/97JB00726.

Wiemer, S., and M. Wyss (2000). Minimum magnitude of completeness in earthquake catalogs: Examples from Alaska, the Western United States, and Japan, *Bull. Seismol. Soc. Am.* **90,** 859–869, doi: 10.1785/0119990114.

Wiemer, S., S. McNutt, and M. Wyss (1998). Temporal and three-dimensional spatial analyses of the frequency-magnitude distribution near Long Valley Caldera, California, *Geophys. J. Int.* **134,** 409–421, doi: 10.1046/j.1365-246x.1998.00561.x.

Wyss, M., F. Klein, K. Nagamine, and S. Wiemer (2001). Anomalously high *b*-values in the south flank of Kilauea Volcano, Hawaii: Evidence for the distribution of magma below Kilauea's east rift zone, *J. Volcanol. Geotherm. Res.* **106,** 23–27, doi: 10.1016/S0377-0273(00)00263-8.

Zaliapin, I., and Y. Ben-Zion (2013a). Earthquake clusters in southern California I: Identification and stability, *J. Geophys. Res.* **118,** no. 6, 2847–2864, doi: 10.1002/jgrb.50179.

Zaliapin, I., and Y. Ben-Zion (2013b). Earthquake clusters in southern California II: Classification and relation to physical properties of the crust, *J. Geophys. Res.* **118,** no. 6, 2865–2877, doi: 10.1002/jgrb.50178Zhuang.

Zaliapin, I., A. Gabrielov, V. Keilis-Borok, and H. Wong (2008). Clustering analysis of seismicity and aftershock identification, *Phys. Rev. Lett.* **101,** no. 1, 1–4, doi: 10.1103/PhysRevLett.101.018501.

Zhuang, J., Y. Ogata, and D. Vere-Jones (2002). Stochastic declustering of space-time earthquake occurrences, *J. Am. Stat. Assoc.* **97,** no. 458, 369–380, doi: 10.1198/016214502760046925.

Manuscript received 16 September 2022
Published online 15 February 2023